ADVANCED MATERIALS
www.advmat.de

Multidimensional Photopatterning of Heterogeneous Liquid-Crystal Superstructures Toward Higher-Level Information Optics

Si-Jia Liu, Yi-Heng Zhang, Rui Sun, Peng Chen, Lin Zhu, Dong Zhu, Wen Chen, Yi-Ming Wang, Shi-Hui Ding, Shi-Jun Ge, Wei Hu,* and Yan-Qing Lu**

Soft matter, featuring superior flexibility and intriguing tunability, has shown enormous potential in sensors, soft robots, and light tailoring. However, limited by its inherent structural complexity, soft matter remains uncompetitive in multidimensional and high-density information optics. Herein, a heterogeneous liquid-crystal (LC) superstructure composed of interlocked nematic and chiral LCs is designed to achieve higher-dimensional light control. Optically multidimensional photopatterning with programmable UV polarization and dosage is proposed to precisely customize both transverse and longitudinal LC arrangements, bringing in a wide range of light-matter interactions within a single micrometer-thick film. The constructed heterogeneous LC superstructure not only enables simultaneous near-field full-color printing and far-field full-color holography but also boasts brightness controllability and polarization selectivity. This low-cost photonic structure enables a high information density of ≈1.6 million hybrid-dimensional optical data per square millimeter, unlocking new capabilities in optical storage, display, and encryption. This work creates an ingenious bond between advanced photopatterning technologies and higher-level optical informatics, and pioneers soft-matter-mediated full-dimensional optics.

1. Introduction

Soft matter occupies a middle ground between ideal fluid and solid,[1] including polymers, colloids, liquid crystals (LCs), surfactants, etc. Owing to the relatively weak interactions among their mesoscopic structural units, these materials commonly show distinctive softness and sensitive responsiveness to external stimuli, such as heat,[2] electric field,[3] light irradiation,[4] and mechanical stress.[5,6] In particular, light is an excellent partner for soft matter. On the one hand, light can be a high-precision controller of soft structures, playing a critical role in constructing crosslinked networks,[7,8] inducing the reconfiguration of soft helices,[9,10] and triggering the motion of soft robots.[11] On the other hand, structured soft matter can reversely manipulate light in various manners, particularly the structural colors via polymers[12,13] and colloids,[14] and commercial spatial light modulators via LCs.[15] However, conventional soft structures are mostly restricted to controlling only the spectrum or the phase dimension of light.

The full utilization of all optical dimensions (amplitude, phase, wavelength, polarization, space, time, etc.) holds great promise for boosting large-capacity and high-security information processing.[16–19] In nature, many species have evolved delicate, heterogeneous photonic structures to leverage multidimensional optical information in their communication, signaling, and camouflage.[20–23] This hints at the key to higher-dimensional light control with soft matter, that is, the higher-degree-of-freedom (DoF) structural manipulation of its building blocks. In this regard, LCs stand out owing to their intrinsic anisotropy, which adds more controllable DoFs to both their structures and optical properties.[24–28] Recently, the manipulation of LCs' azimuthal orientation has cultivated impressive functions based on the geometric phase,[29–32] such as structured light tailoring,[33] multiplexed holography,[34] and optical edge detection.[35,36] However, limited by LCs' inherent structural complexity and flexibility, the full exploitation of their structural DoFs has remained elusive, significantly impeding higher-dimensional light control in soft matter systems.

In this work, we propose a multidimensional photopatterning strategy to break through the long-standing DoF limitation in both soft structure manipulation and its resultant light control. A heterogeneous LC superstructure is designed and constructed by associating the self-assembly of chiral LC (CLC) nanohelices with a top-down wash-out/refill process. Through the so-called multidimensional photopatterning with the aid of optical

S.-J. Liu, Y.-H. Zhang, R. Sun, P. Chen, L. Zhu, D. Zhu, W. Chen, Y.-M. Wang, S.-H. Ding, S.-J. Ge, W. Hu, Y.-Q. Lu
National Laboratory of Solid State Microstructures
Key Laboratory of Intelligent Optical Sensing and Manipulation
College of Engineering and Applied Sciences, and Collaborative Innovation Center of Advanced Microstructures
Nanjing University
Nanjing 210093, China
E-mail: chenpeng@nju.edu.cn; huwei@nju.edu.cn; yqlu@nju.edu.cn

The ORCID identification number(s) for the author(s) of this article can be found under https://doi.org/10.1002/adma.202506778

DOI: 10.1002/adma.202506778

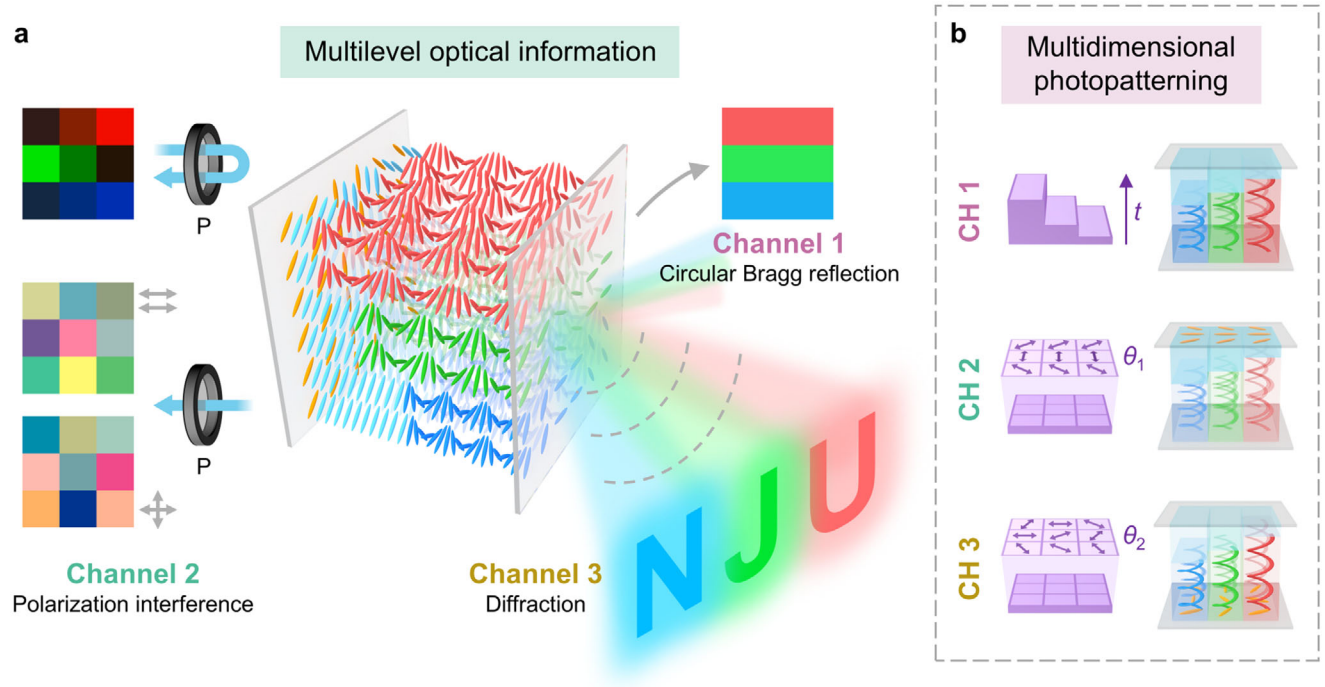

Figure 1. Heterogeneous LC superstructure via multidimensional photopatterning for multilevel optical encoding. a) Multilevel optical information encoded in an interlocked LC superstructure. Red, green, and blue (RGB) rods represent CLC molecules with different photonic bandgap (PBG). Pale blue rods represent NLC molecules. Channel (CH) 1 contains patterned Bragg reflection colors decrypted with the naked eye. CH 2 contains various reflective brightness (upper) and transmissive polarization interference colors (lower) decrypted with polarizers (double-ended arrows). CH 3 contains full-color holography decrypted with a laser. b) Schematic illustration of multidimensional photopatterning. By programming the exposure time (t) and polarization directions (θ_1 and θ_2) of UV light, optical information for CH 1 to CH 3 is encoded into three different parts of the heterogeneous LC superstructure (respectively highlighted). Helices in RGB blocks represent the CLC superstructures with different PBG. Pale blue blocks represent the NLCs. Yellow rods indicate the surface alignment of LCs.

multidimensionality, its supramolecular structure is precisely tailored both transversely and longitudinally, either in the form of a tunable cell or a flexible film. Such higher-DoF structural control of LCs can activate higher dimensions of light, thus allowing the high-density encoding of multilevel optical information, including full-color printing, brightness variation, and polarization interference colors in the near-field, and spin-selective full-color holography in the far-field. This work facilitates the exquisite construction of LC superstructures, enlightens multiplexed information optics, and provides an unprecedented paradigm for full-dimensional soft matter photonics.

2. Results

2.1. Principle of Multilevel Optical Encoding via Multidimensional Photopatterning

To activate higher optical dimensions in soft matter, we propose a delicate heterogeneous LC superstructure (**Figure 1a**) and develop a new strategy for multilevel optical information encoding (Figure 1b), uncovering the interrelation among fabrication techniques, soft structure DoFs, optical dimensions and multilevel information optics (Figure S1, Supporting Information). In the proposed heterogeneous superstructure, two different LC phases, i.e., nematic LCs (NLCs) and CLCs, are interlocked in a single cell, with their uneven interface resembling a surface relief (Figure 1a). The NLCs, arranged by surface anchoring and intermolecular interaction, function like an inhomogeneous waveplate to conduct diverse polarization conversions. While for the CLCs, their self-assembled helical nanostructure can present various fade-resistant structural colors due to the circular-polarization-selective Bragg reflection within the photonic bandgap (PBG, Figure S2a, Supporting Information).[37–39] Since PBG spans the wavelength range $n_o p$–$n_e p$ theoretically (n_o/n_e denoting the ordinary/extraordinary refractive index, and p denoting the helical pitch), the delicate spatial programming of p can lead to space-variant PBG and reflection colors. Moreover, the reflected light from CLCs will gain an additional geometric phase that is twice their surface alignment angle owing to the spin-orbit interaction of light.[40,32] Hence, arbitrary phase manipulation and consequent diffractive functions can be attained within PBG via proper surface patterning of CLCs. See a more detailed explanation of the principle in Section S1 (Supporting Information).

To encode multilevel optical information with ultra-high density, we propose a processing strategy called multidimensional photopatterning and ingeniously incorporate it into a wash-out/refill process (Figure 1b). Notably, in this context, the term "multidimensional" refers to the optical multidimensionality of UV exposure, different from the spatial dimensions associated with conventional 2D/3D photolithography. Compared to the common UV lithography, the proposed multidimensional

photopatterning not only controls the dosage of UV exposure, but also controls its pixelated linear polarization directions. First, we find that by varying the exposure time (t) spatially, we can obtain CLC nano-helices with different heights and thus different p, creating patterned Bragg reflection colors observable with the naked eye or under an optical microscope (Channel (CH) 1 in Figure 1a,b). Second, through UV exposure of space-variant linear polarization angles (θ_1), the NLC molecules can be guided by the polarization-sensitive photoalignment agent and align perpendicularly to the UV polarization ($\theta_1 + 90°$). Thanks to NLCs' polarization converting ability, brightness-tunable reflection colors and abundant transmission colors can be expected under polarizers (CH 2 in Figure 1a,b) due to the polarization interference of light (Figure S2b, Supporting Information). Third, the surface alignment of the CLC helices ($\theta_2 + 90°$) can also be customized through another polarized photopatterning process (θ_2). With space-variant PBG, independent geometric phases and diffractive functions (Figure S2c, Supporting Information) can be encoded for separate wavelengths, enabling wavelength-multiplexed applications such as the far-field full-color holography (CH 3 in Figure 1a,b). CH 1 to CH 3, each with additional spectral subchannels, can only be correctly retrieved under appropriate conditions (Figure 1a), providing a high-security strategy for multilevel optical storage and encryption.

2.2. Full-Color Printing via Surface-Relief-Embedded Chiral Superstructures

The secret to various reflection colors in CH 1 lies in our discovery of the photo-induced non-uniform swelling of CLC helices (**Figure 2**a,b). First, the right-handed CLC/reactive monomer mixture was infiltrated into a uniformly aligned cell to form self-assembled helical nanostructures, exhibiting circular-polarization-selective high reflectance and good planar texture (Figure 2c). Then, the mixture was polymerized by UV light to stabilize the nano-helices (Figure 2a; Figure S3, Supporting Information). Afterward, nonreactive components were washed out by immersing the cell in acetone, leaving only a shrunk cholesteric polymer scaffold with a large number of nano-pores (see scanning electron microscope (SEM) images in Figure S4, Supporting Information). Pixelated UV exposure with various exposure times (t) was then conducted on the scaffold through a dynamic-mask photopatterning system, which could alter the local swelling ability of the sponge-like scaffold. At last, the cell was refilled with NLCs, upon which LC molecules quickly entered the porous scaffold and stretched the CLC helices. The regions that had been illuminated for a longer time tended to swell to a lower height (i.e., smaller p and shorter-wavelength PBG; Figure 2a), which can be plausibly explained by the denser crosslinking induced by larger exposure dosage.[41] Consequently, the interface between CLCs and NLCs got uneven, just like a surface relief, and the final PBG of CLCs varied spatially according to the local t. See more details about materials and fabrication in the Experimental Section.

Figure 2d,e presents the measured relation between PBG and t, guiding our way toward customized full-color printing. As an explicit example, a rainbow-like sample fabricated with gradient t is demonstrated in Figure 2b, whose color gamut (inset of Figure 2e) evidences the large programmable range of colors. Moreover, the wash-out/refill process allows for multifunctional optical encryption with good recyclability. As verified by the "ginkgo" sample in Figure 2f, optical information can be concealed in the transparent scaffold, and decrypted either temporarily or durably according to the volatility of the refilling substance. When refilled with acetone, the ginkgo pattern appears in blue owing to the refractive index change and pitch variation of the CLC structure. This pattern lasts only a few minutes and then totally disappears due to the evaporation of acetone (see intermediate process in Figure S5a and Movie S1, Supporting Information). Other solvents, such as dimethylformamide (DMF), can also be used to decrypt the same pattern in different colors (see more results of refilling with different solvents in Figure S6, Supporting Information). When refilled with NLCs, the revealed ginkgo pattern exhibits fine shapes with three different colors, which still remain stable after 30 days (Figure 2f). Besides, this soft superstructure also boasts good external-field tunability, showing unique thermochromic (Figure 2f; Movie S2, Supporting Information) and electrochromic (Figure S5b, Supporting Information) properties. To further verify the ultra-high printing precision, we designed another pattern, "the nine-colored deer", with fruitful colors, complex lines, and various shapes (Figure 2g). The corresponding sample showcases micro-scale linewidth, sharp edges, and inconspicuous color crosstalk, agreeing perfectly with the initial design.

2.3. On-Demand Programming of Brightness and Polarization Interference Colors

On the essential basis of full-color printing, we further introduce the polarized photopatterning to liberate new optical dimensions. **Figure 3**a illustrates the complete fabrication process. The linearly polarized UV exposure before filling with CLCs (θ_2) was aimed at controlling the CLC surface alignment, while the second polarized exposure before refilling (θ_1) was aimed at aligning the refilled NLCs (see the Experimental Section for more details). After fabrication, NLCs and CLCs were integrated as a micrometer-thick film with controllable relative thickness (Figure 3b) and customizable independent alignments.

First, optical effects brought by the variably-aligned NLCs ($\theta_1 + 90°$) are explored. As shown in Figure 3c, light propagation in the heterogeneous LC superstructure includes four typical cases, where three physical mechanisms are variously combined according to the light's propagation direction. NLCs can convert polarization states diversely according to their alignment and retardance, albeit with dispersion. When CLCs are involved together, their circular Bragg reflection and optical rotatory power[42,43] further contribute to the wavelength-dependent polarization conversions, leading to more complex spectral performances under polarizers (see detailed analysis in Section S1, Supporting Information). To demonstrate this, we fabricated a 390-piece superstructure with 13 discrete θ_1 (−90° to 90°, spaced by 15°), 30 different t (same as Figure 2b), and a uniform θ_2. On the reflection side with parallel polarizers (CH 2-1; Figure 3d), this superstructure achieves the high-contrast brightness manipulation of rainbow-like Bragg reflection colors, agreeing well with the simulation

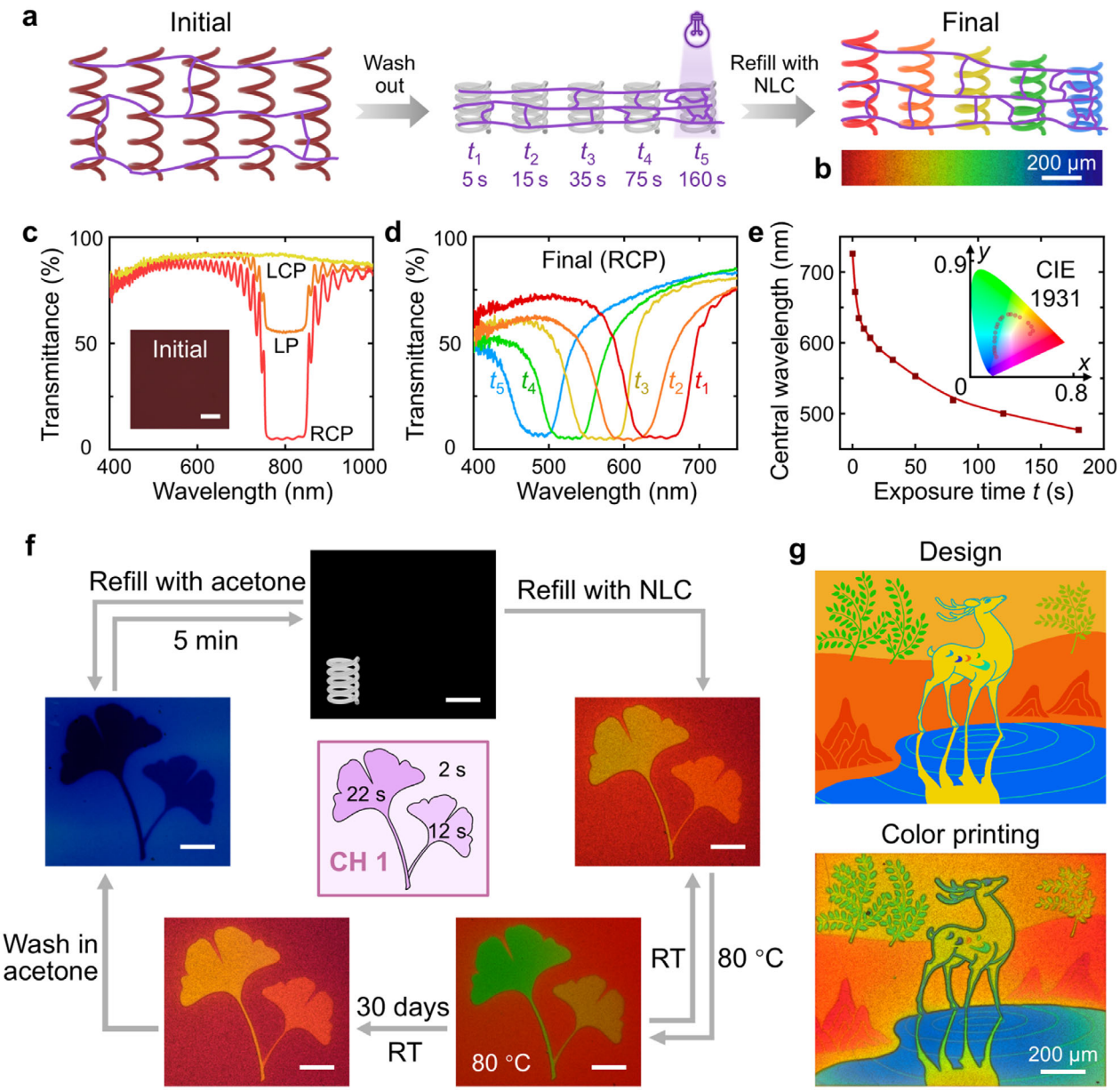

Figure 2. Recyclable high-resolution full-color printing by programming UV exposure time (t). a) Patterning of Bragg reflection colors in CH 1 through space-variant UV exposure time (t_1–t_5). Colorful helices represent the CLC superstructures in different fabrication stages. Purple lines represent the crosslinked polymer networks, which get denser after UV exposure. b) Reflective micrograph of the rainbow-like color printing. c) Initial transmittance spectra with left circularly polarized (LCP), linearly polarized (LP), and right circularly polarized (RCP) incident light. Inset is the initial micrograph. d) Final transmittance spectra with RCP incidence for different exposure times (t_1–t_5). e) Dependence of the PBG central wavelength on the exposure time t. Inset is the color gamut of the rainbow-like color printing mapped on the CIE 1931 chromaticity diagram. f) Recyclable and thermochromic color printing of ginkgo leaves with two distinct decryption modes (temporary or durable). The corresponding distribution of t is provided in the center. RT, room temperature. g) Design and micrograph of the delicate full-color printing, "the nine-colored deer". All scale bars represent 200 μm.

(see details in Section S2 and Figure S7, Supporting Information). Meanwhile, on the transmission side with parallel (CH 2-2; Figure 3e) or orthogonal polarizers (CH 2-3; Figure 3f), numerous polarization interference colors are vividly created, showing unprecedented diversity of soft-matter-mediated structural colors.

Such a 390-piece superstructure can serve as a look-up table for the on-demand programming of brightness and colors (Figure 3d–f; see its dependence on polarizer/analyzer directions in Figures S8 and S9, Supporting Information). Accordingly, a butterfly sample was prepared with red, orange, green, blue, and black colors in CH 2-1, where the black color is actually the red at zero brightness (Figure 3g). In CH 2-2 or CH 2-3, the butterfly wings exhibit various polarization interference colors (Figure 3h). For another sample, full-color (i.e., red, green, and blue (RGB)) geometric shapes can be observed in CH 1 (Figure 3i).

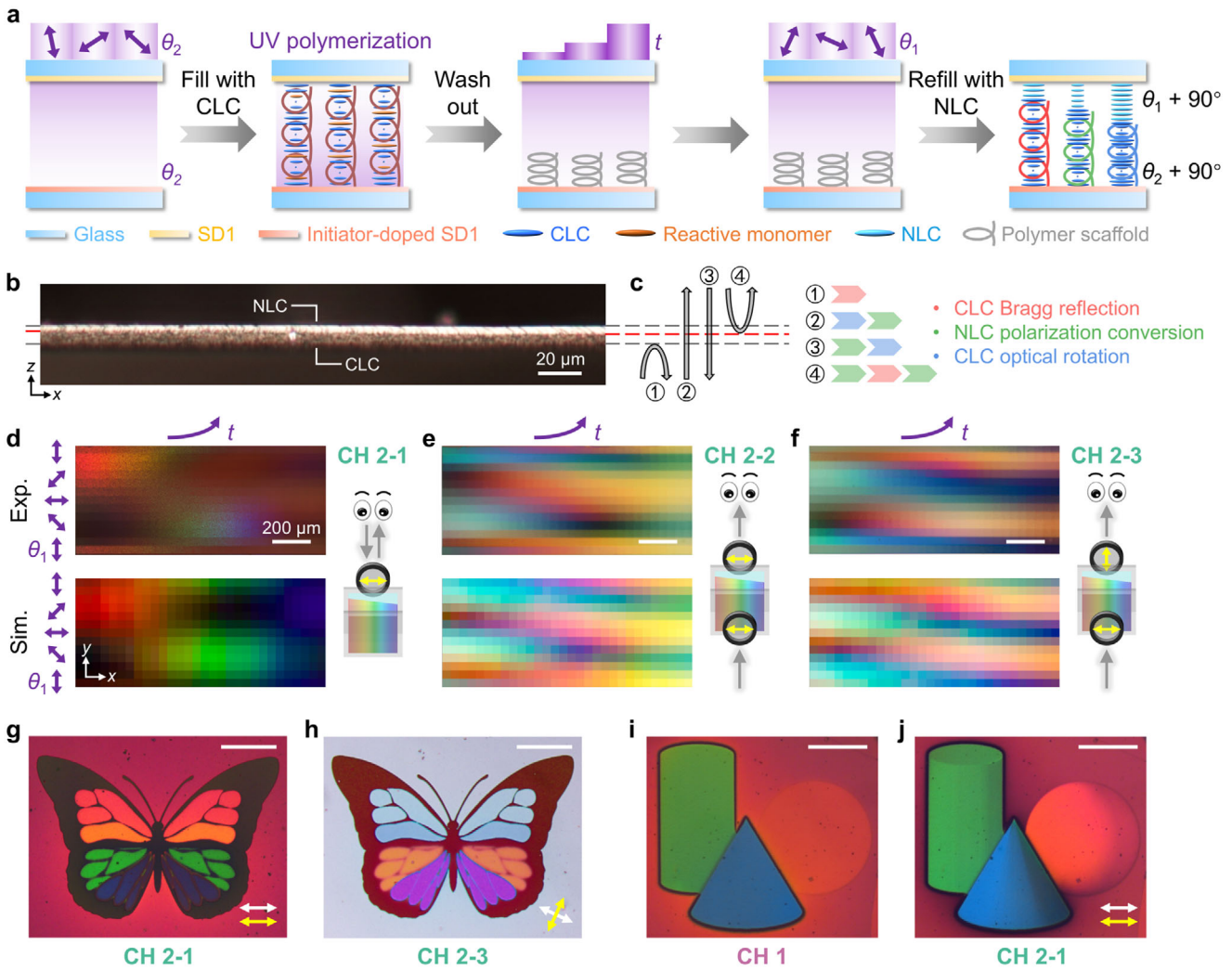

Figure 3. Patterned brightness and polarization interference colors achieved by programming UV polarization direction (θ_1). a) Complete fabrication process of the heterogeneous LC superstructure, where θ_2, t, and θ_1 are encoded successively in different stages. SD1 is adopted as the photoalignment agent and is doped with the photoinitiator on only one substrate to tether the polymer scaffold. b) Cross-sectional micrograph of the heterogeneous LC superstructure, where the thickness of NLC/CLC changes along the x axis (labeled by lines on the left and right sides). The scale bar represents 20 μm. c) Schematic of four typical cases of light transmission/reflection in the LC superstructure, along with the respective physical mechanisms involved. d–f) Experimental (upper) and simulated (lower) polarized micrographs of a 390-piece superstructure fabricated with various photopatterning parameters t and θ_1. Schematics on the right illustrate the respective observation methods of (d) CH 2-1, (e) CH 2-2, and (f) CH 2-3. Yellow arrows depict the transmission axes of polarizers/analyzers. Gray arrows depict the propagation directions of light. g,h) Micrographs of a butterfly sample in (g) CH 2-1 and (h) CH 2-3. White and yellow arrows represent the polarizing and analyzing directions, respectively. i,j) Micrographs of a geometric object sample in (i) CH 1 and (j) CH 2-1, where the pattern in CH 2-1 is much more vivid due to brightness variation. All scale bars in (d–j) represent 200 μm.

Interestingly, via the variant control of NLC alignment, shades can be introduced to these shapes in CH 2-1 (Figure 3j), making for a much more vivid pattern of three-dimensional objects. Such brightness controllability breaks the limitation of mere color variation in conventional LC structural colors.

2.4. Geometric Phase Manipulation Compatible with Diverse Coloration

Leveraging CLCs' capability of geometric phase manipulation, the fascinating combination of near-field color printing and far-field diffractive functions can be expected. Theoretically, the CLC geometric phase is reliant on the incident light helicity, the CLC chirality, and the CLC surface alignment (θ_2 + 90°). Taking the used right-handed CLCs for example, only the right circular polarization (RCP) of incident light can be Bragg reflected within PBG, while the left circular polarization (LCP) and light outside PBG will directly transmit. With preserved right-handed helicity, the reflected RCP light will derive an additional geometric phase[29] which is twice the CLC surface alignment angle (**Figure 4a**), and then various diffractive functions, such as lensing, beam steering, and holography, can occur.

According to the above principle, we calculated a pure-phase hologram of butterflies (inset of Figure 4a) using the Gerchberg–Saxton (G–S) algorithm, and encoded it into the CLC alignment

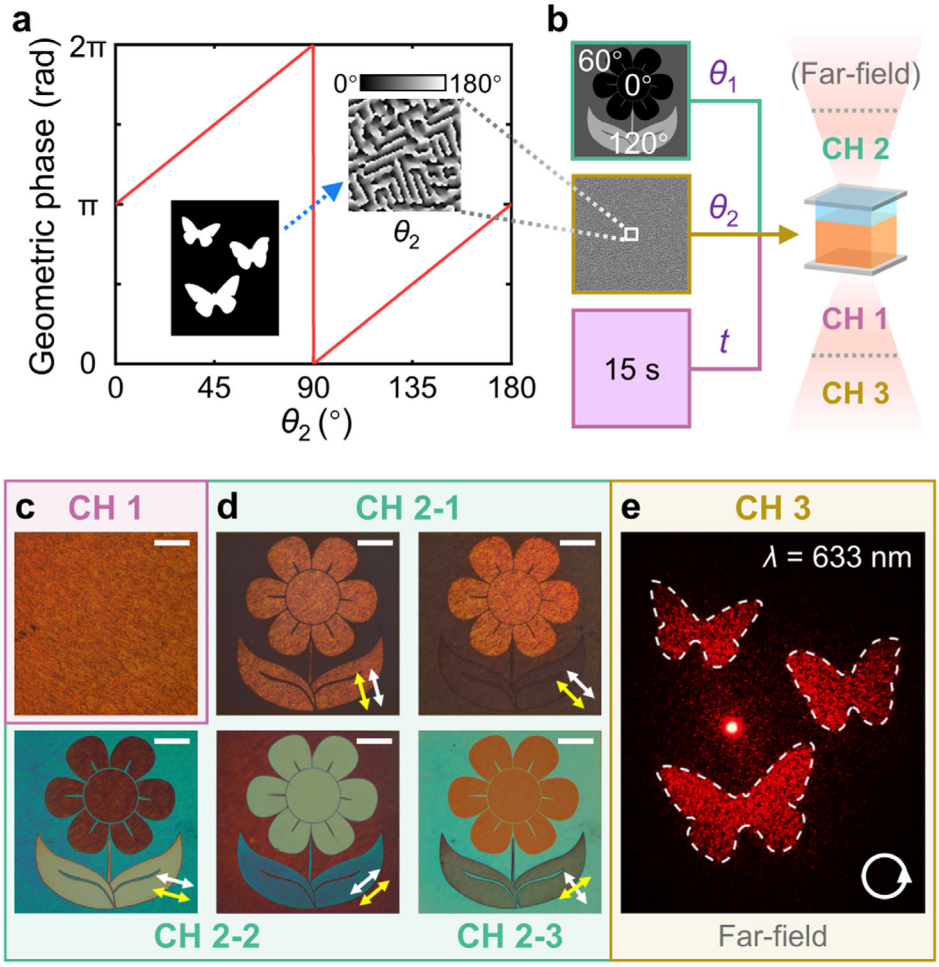

Figure 4. Synchronous near-field printing and far-field holography by programming two-stage UV polarization directions (θ_1 and θ_2). a) Theoretical relation between the CLC geometric phase and θ_2. The inset illustrates the calculation of the hologram-encoded θ_2 from the target holographic image. b) Designed photopatterning parameters (θ_1, θ_2, and t) for the near- and far-field multiplexed LC superstructure. The sophisticated distribution of θ_2 is enlarged in the inset of (a). The schematic on the right vividly illustrates the near-field (CH 1 and CH 2) and far-field (CH 3) multiplexing. c) Micrograph of the sample in CH 1. d) Polarized micrographs of the sample in CH 2-1, CH 2-2, and CH 2-3. White and yellow arrows depict the various polarizing and analyzing directions. e) Holographic butterfly image reconstructed in CH 3 with RCP incidence at 633 nm. The white arrowed circle indicates the incident polarization. All scale bars represent 200 μm.

of a heterogeneous LC superstructure. The parameters for the multidimensional UV photopatterning are shown in Figure 4b, including a flower-shaped θ_1, a hologram-encoded θ_2, and a uniform t. As illustrated above, t and θ_1 account for CH 1 and CH 2 in the near-field, while θ_2 is responsible for the diffractive channel CH 3 in the far-field. For the fabricated sample, an orange color originating from uniform Bragg reflection is obtained in CH 1 (Figure 4c), while flower-shaped patterns of brightness or polarization interference colors are abundantly observed in CH 2 (Figure 4d; see more results in Figure S10 and Movie S3, Supporting Information). When illuminated by RCP laser from the CLC side, this superstructure further reconstructs the holographic image of butterflies in CH 3 (Figure 4e) at a diffraction distance of 50 cm. The simultaneous near- and far-field display greatly extends traditional LC structural coloration by manipulating the new independent dimension of phase, unveiling the good compatibility between multiple optical dimensions in the proposed heterogeneous superstructures.

2.5. Heterogeneous LC Superstructure for Higher-Level Information Optics

With full exploitation of CH 1 to CH 3, the proposed heterogeneous LC superstructure is able to tailor six optical dimensions simultaneously, including wavelength, polarization, amplitude, phase, direction, and space, thus holding great prospects for higher-level information optics (**Figure** 5a; see details in Figure S11, Supporting Information). As a proof-of-concept demonstration, we customized a multilevel encrypted superstructure: a full-color flower pattern in CH 1, a line of poem in CH 2, and a full-color butterfly image in CH 3 (Figure 5a). Figure 5c shows the corresponding UV photopatterning parameters. Notably, θ_2 was specially designed by merging three distinct phase hologram pieces, respectively linked to RGB subchannels (Figure 5b). For each subchannel, the corresponding hologram piece was optimized given the target near-field amplitude pattern and far-field holographic image (see design details in Section S3 and

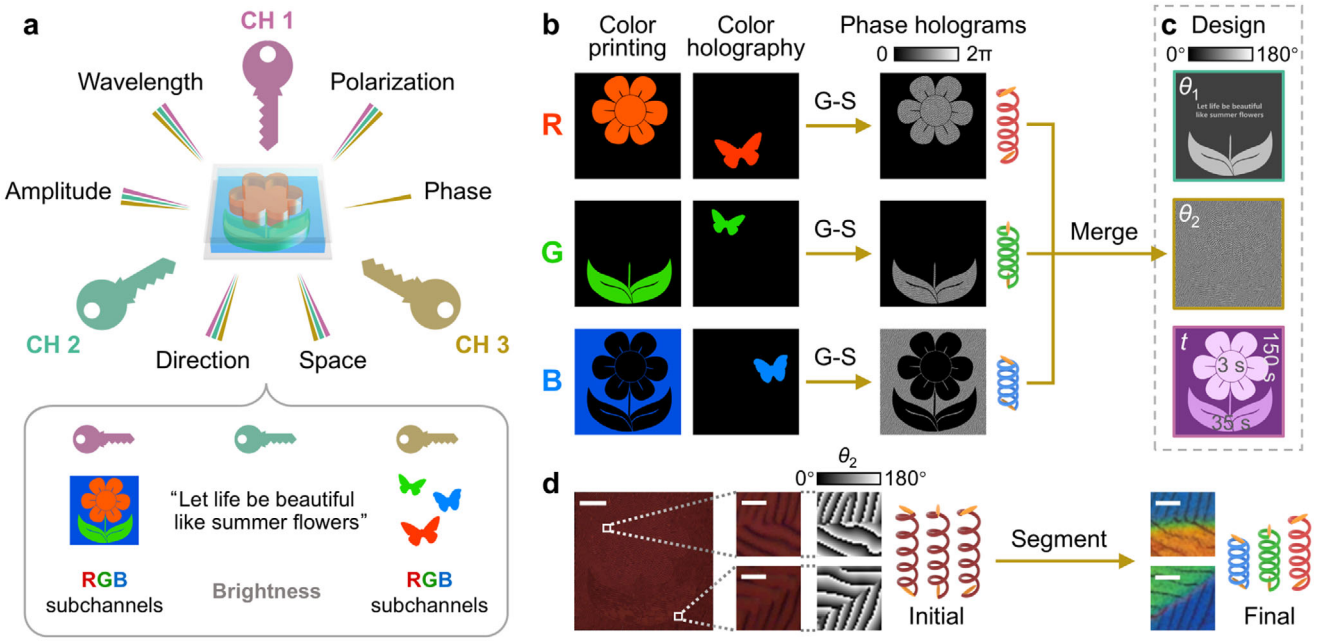

Figure 5. Higher-dimensional and higher-level optical encryption. a) Schematic illustration of encrypting multilevel optical information regarding 6D into a heterogeneous LC superstructure. The relation between optical dimensions and CH 1, CH 2, and CH 3 is labeled by the number and colors of lines (upper). The multilevel optical information and related subchannels are listed in the box (lower). b) Derivation of the three hologram pieces for RGB subchannels, which constitute the hologram-encoded θ_2. G–S, the Gerchberg–Saxton algorithm. RGB helices with differently oriented yellow rods represent the target CLC superstructures with independent PBG and surface alignment. c) Designed photopatterning parameters (θ_1, θ_2, and t) for the multilevel optical encryption. d) Normal-sized and enlarged reflective micrographs of the LC superstructure before and after segmenting, and the enlarged θ_2 distribution. Colorful helices represent the initial and final CLC superstructures. The scale bar in the left micrograph represents 200 μm, and all the other scale bars in the enlarged micrographs represent 20 μm.

Figure S12, Supporting Information). In the fabrication process, these hologram pieces were synchronously encoded into the CLC alignment (Figure 5d) during the first polarized photopatterning (θ_2). Owing to the spatial variance of t, the LC superstructure was finally segmented into RGB regions, exhibiting high precision, sharp edges (below 5 μm in width), and negligible color crosstalk (Figure 5d).

The multilevel optical decryption of this heterogeneous superstructure is shown in **Figure 6a–d**. First, the preprogrammed full-color printing is disclosed with fine micro-scale details (CH 1; Figure 6a). The relative reflection spectra of its RGB regions are respectively measured under orthogonal circular polarizers, in which the high reflection for RCP and the near-zero reflection for LCP verify the strong spin selectivity (Figure 6b). Second, the encrypted poem is revealed by inserting linear polarizers (CH 2; Figure 6c). Taking CH 2-1 for example, the poem line in black is easily distinguished from the bright background. Third, with polychromatic laser illumination, RGB butterfly images can be reconstructed independently in the far-field, achieving the high-quality hybrid-multiplexed full-color holography (CH 3; Figure 6d). Moreover, we can optionally stabilize such a multilevel encrypted LC superstructure to form a flexible free-standing film, through refilling with LC reactive monomers, thoroughly polymerizing with UV light, and then peeling off the substrates (Figure 6e). The fabricated all-polymer functional optical film can be concealed under an LCP filter and revealed under an RCP filter (Figure 6f; see more results in Figure S13 and Movie S4, Supporting Information), presenting the unique spin-selective invisibility. Only with proper decryption methods can the respective optical information in CH 1, CH 2, and CH 3 be decrypted, which offers a prototype for one-to-many encrypted communication and multilevel anticounterfeiting labels (Figure S14, Supporting Information), and provides a versatile platform for large-capacity and high-security information optics.

The proposed multidimensional photopatterning provides a high-precision, low-cost, and convenient approach for customizing LC soft structures. Leveraging this method, we can design and construct exquisite heterogeneous LC superstructures with a high spatial resolution of 18578 dots per inch (DPI) for each of the three independent channels, enabling a high information density of ≈1.6 million data units per square millimeter (Experimental Section). Such LC superstructures drastically exceed the optical dimensions of conventional soft matter while preserving the merits of flexibility and external-field controllability, achieving four-dimensional optical holographic multiplexing in terms of near/far field, polarization, incident direction, and wavelength. The ingenious integration of structural colors, variant brightness, and geometric phases allows for high-capacity optical storage and high-security encryption. To further enhance its capacity, more wavelength and polarization channels can be established through segmenting and stacking. Besides, the angle-dependent coloration is observed (Figure S15, Supporting Information), suggesting a new manipulable dimension. The interleaved design[44] and color mixing scheme[45] can also be used to achieve better diffractive performances and richer color combinations. Moreover, the proposed heterogeneous LC

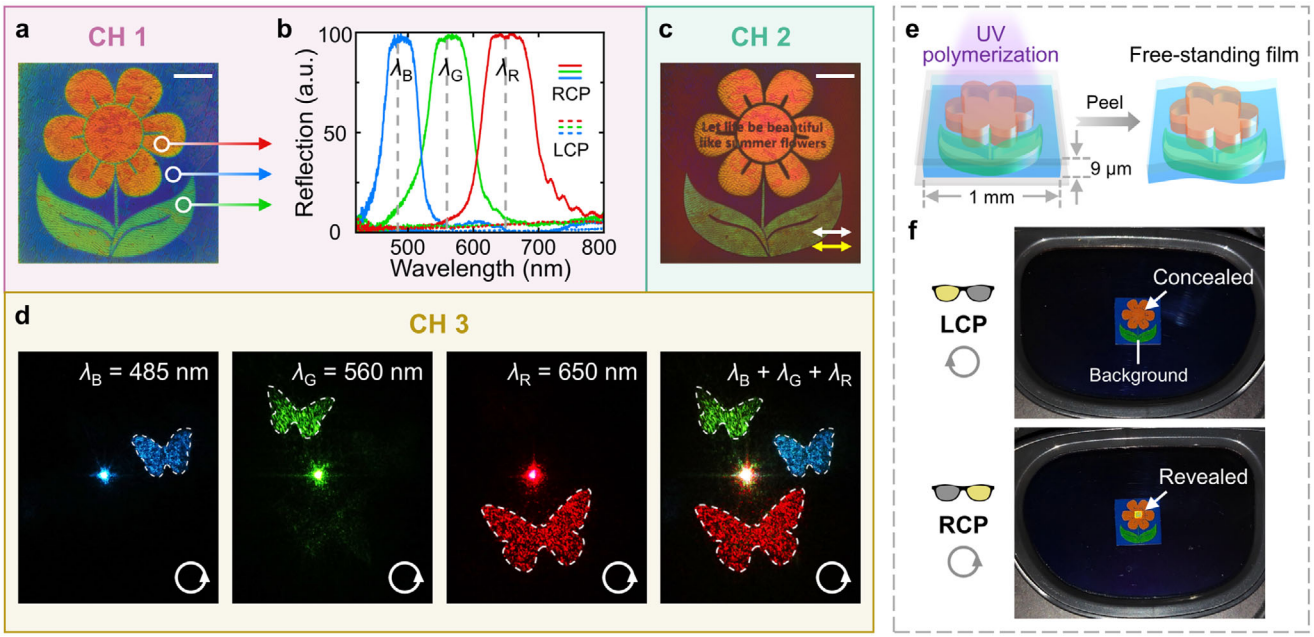

Figure 6. Multilevel optical decryption of the heterogeneous LC superstructure and its formation as a free-standing film. a) Micrograph of the multilevel encrypted sample in CH 1. b) Reflection spectra for the circled RGB regions in (a) with RCP (solid lines) and LCP (dashed lines) incidence, respectively. Three particular wavelengths (λ_B = 485 nm, λ_G = 560 nm, and λ_R = 650 nm) are marked by vertical lines. c) Polarized micrograph of the sample in CH 2-1. White and yellow arrows represent the horizontal polarizer and analyzer. d) Wavelength-multiplexed full-color holography of butterflies decrypted in CH 3 with RCP laser (white arrowed circles). The respective incident wavelengths are labeled in the upper right. e) Formation of a multilevel encrypted free-standing optical film from the heterogeneous LC superstructure. f) Photos of the formed free-standing film under LCP (upper) and RCP (lower) filters of 3D glasses. The same flower pattern printed on the paper (1 cm × 1 cm) is used as the background. All scale bars represent 200 μm.

superstructure can be easily extended to many other wavelength-dependent functionalities, such as achromatic lensing, color display, and multiplexed optical computing. Orbital angular momentum of light, as another important optical dimension, can be further introduced to achieve richer functions and higher-level optical informatics. Such subtle interplay between light and soft matter is expected to open up new avenues in active and smart optics.

3. Conclusion

In summary, we have established the delicate interconnections among photopatterning dimensions, soft structure DoFs, optical dimensions, and multilevel information optics. Through combining chiral self-assembly, multidimensional photopatterning, and a wash-out/refill process, NLCs and CLCs are interlocked in a single cell with customized transverse microstructures and longitudinal nanostructures. The transverse alignments of heterogeneous LCs are independently guided for on-demand polarization conversion and geometric phase manipulation. Meanwhile, the longitudinal CLC nano-helices are stretched to different heights, inducing the space-variant PBG. This LC superstructure not only enables simultaneous full-color printing and holography but also boasts brightness controllability and spin selectivity, greatly enhancing the versatility of LC devices. According to the refilling substance, the optical functionalities can be arbitrarily chosen as temporary or durable, and tunable or stable. This work promotes the ingenious building of soft-matter superstructures, unveils their unprecedented capabilities in full-dimensional light control, and offers an important glimpse into their great potential in next-generation encryption, display, and computing.

4. Experimental Section

Materials: The photoalignment agent SD1 was dissolved in DMF at a concentration of 0.35 wt.%. The photoinitiator-doped SD1 was a mixture of the SD1 solution with 0.15 wt.% diphenyl ketone. SD1 molecules tended to reorient their absorption oscillators perpendicular to the linear polarization direction of UV exposure, and then guided LC molecules to align parallel to them. The initial right-handed CLC/reactive monomer mixture contained NLC E7 (HCCH, China), right-handed chiral dopant R5011 (HCCH, China), and LC reactive monomer RM257 (HCCH, China) at a weight ratio of 78.1:1.9:20, which could form the porous cholesteric polymer scaffold. Notably, R5011 could be substituted with the left-handed chiral dopant S5011, which would reverse the CLC chirality. The refilling substance for the temporary decryption mode was acetone or DMF, and that for the durable decryption mode was NLC E7, which could enter the nano-pores in the scaffold and induce its swelling. For the free-standing optical film, the refilling substance was the mixture of RM257 and diphenyl ketone at a weight ratio of 95:5. See chemical structures of SD1, diphenyl ketone, RM257, and R5011 in Figure S16 (Supporting Information).

Sample Fabrication: Two ITO glass substrates after UV-Ozone cleaning were spin-coated with photoalignment layers of either SD1 or photoinitiator-doped SD1. After curing at 100 °C for 10 min, a photoinitiator-free substrate was assembled with another photoinitiator-doped substrate to form a 9 μm-thick cell. A wash-out/refill process was then implemented in the cell (Figure 3a), and multidimensional photopatterning was conducted during this process. The multidimensional photopatterning was realized by a digital-micromirror-device-based dynamic-mask photopatterning system,[32] which could arbitrarily control the polarization, dosage, and pattern of UV exposure. The spatial resolution of

multidimensional photopatterning is 1.3672 μm·pixel^{-1}, i.e., 18578 dots per inch (DPI) for each of three independent channels, corresponding to an equivalent DPI of 55734. The information density is ≈1.6 million data units per square millimeter, derived from 534988 pixels·mm^{-2} with triple-channel independent encoding. First, polarized photopatterning (365 nm, 0.54 mW·mm^{-2}, 7.5 s) was carried out with space-variant linear polarization directions θ_2. After filling with the CLC mixture, the CLC molecules at the surface were guided by the SD1 layers, acquiring the surface alignment $\theta_2 + 90°$. Then, the cell was exposed to non-polarized UV light (365 nm, 0.06 mW·mm^{-2}) for 15 min from the photoinitiator-doped side for surface-initiated polymerization. Afterward, the cell was immersed in acetone for 12 h to wash out the nonreactive components. After the evaporation of acetone, only a shrunk polymer scaffold tethered to the photoinitiator-doped substrate was left. Photopatterning (365 nm, 1.58 mW·mm^{-2}) with space-variant exposure time t was then conducted on the scaffold, which could determine the final PBG of CLC helices. After that, the second polarized photopatterning (365 nm, 0.54 mW·mm^{-2}, 7.5 s) was carried out with space-variant polarization directions θ_1. At last, the cell could be refilled with various refilling substances, such as acetone, NLCs, and LC reactive monomers. Notably, when refilling with NLCs at 72 °C, the NLC molecules were guided by the overwritten SD1 layer, acquiring the surface alignment $\theta_1 + 90°$. The free-standing optical film was fabricated by refilling with LC reactive monomers, polymerizing with UV light (365 nm, 0.19 mW·mm^{-2}) for 10 min, and then peeling off the substrates.

Characterizations: All data were measured at room temperature except the thermochromic color printing. All micrographs were captured by a polarized optical microscope (Ci-POL, Nikon, Japan) either in the reflective or transmissive mode. CH 2-1 was captured in the reflective mode with parallel polarizers. CH 2-2 and CH 2-3 were captured in the transmissive mode with parallel and orthogonal polarizers, respectively. To capture the cross-sectional micrograph of the heterogeneous LC superstructure, fully polymerized NLCs were used, and the LC film was carefully fractured. All transmittance spectra were measured by a spectrometer (PG2000-Pro-EX, Ideaoptics, China) with a halogen light source (iDH2000H-HP, Ideaoptics, China). The color gamut in Figure 2e was measured by a spectrometer (PG2000-Pro-EX, Ideaoptics, China) integrated with the microscopy system. The precise temperature control was conducted by a hot stage (LTS120E, Linkam, UK). For holography, a supercontinuum fiber laser (SuperK EVO, NKT Photonics, Denmark) was utilized to generate polychromatic laser beams, which were filtered at different wavelengths by a multi-channel acousto-optic tunable filter (SuperK SELECT, NKT Photonics, Denmark). The far-field holographic images were projected onto a black screen located 50 cm away from the sample to ensure sufficient diffraction distance, and captured by a visible digital camera (EOS M100, Canon, Japan). The optical power of UV exposure was detected by a digital optical power meter (PM100D, Thorlabs, USA).

Supporting Information

Supporting Information is available from the Wiley Online Library or from the author.

Acknowledgements

This work was supported by the National Key R&D Program of China (Nos. 2021YFA1202000, and 2022YFA1203700), the National Natural Science Foundation of China (NSFC) (Nos. T2488302, 62222507, 62035008, 62175101, and 624B2065), the Innovation Program for Quantum Science and Technology (No. 2021ZD0301500), the Fundamental Research Funds for the Central Universities (No. 021314380273), the Natural Science Foundation of Jiangsu Province (No. BK20243067), and the Postgraduate Research & Practice Innovation Program of Jiangsu Province (No. KYCX23_0142).

Conflict of Interest

The authors declare no conflict of interest.

Data Availability Statement

The data that support the findings of this study are available from the corresponding author upon reasonable request.

Keywords

chiral structures, holography, liquid crystals, optical multiplexing, structural colors

Received: April 9, 2025
Revised: May 13, 2025
Published online:

[1] M. Doi, *Soft Matter Physics*, 1st Edition, Oxford University Press, Oxford, UK **2013**.
[2] T. H. Ware, M. E. McConney, J. J. Wie, V. P. Tondiglia, T. J. White, *Science* **2015**, *347*, 982.
[3] S. J. Liu, L. Zhu, Y. H. Zhang, W. Chen, D. Zhu, P. Chen, Y. Q. Lu, *Adv. Mater.* **2023**, *35*, 2301714.
[4] Z. Zheng, H. Hu, Z. Zhang, B. Liu, M. Li, D.-H. Qu, H. Tian, W.-H. Zhu, B. L. Feringa, *Nat. Photonics* **2022**, *16*, 226.
[5] B. H. Miller, H. Liu, M. Kolle, *Nat. Mater.* **2022**, *21*, 1014.
[6] R. R. Sahu, A. S. Ramasamy, S. Bhonsle, M. Vailshery, A. S Kumar, T. D. Gupta, *Nat. Nanotechnol.* **2024**, *19*, 766.
[7] Y. Geng, R. Kizhakidathazhath, J. P. F. Lagerwall, *Nat. Mater.* **2022**, *21*, 1441.
[8] S. H. Choi, J.u H. Kim, J. Ahn, T. Kim, Y. Jung, D. Won, J. Bang, K. R. Pyun, S. Jeong, H. Kim, Y. G. Kim, S. H. Ko, *Nat. Mater.* **2024**, *23*, 834.
[9] Z. G. Zheng, Y. Li, H. K. Bisoyi, L. Wang, T. J. Bunning, Q. Li, *Nature* **2016**, *531*, 352.
[10] P. Chen, L.-L. Ma, W. Hu, Z.-X. Shen, H. K. Bisoyi, S.-B.o Wu, S.-J. Ge, Q. Li, Y.-Q. Lu, *Nat. Commun.* **2019**, *10*, 2518.
[11] A. H. Gelebart, D. J. Mulder, M. Varga, A. Konya, G. Vantomme, E. W. Meijer, R. L. B. Selinger, D. J. Broer, *Nature* **2017**, *546*, 632.
[12] M. M. Ito, A. H. Gibbons, D. Qin, D. Yamamoto, H. Jiang, D. Yamaguchi, K. Tanaka, E. Sivaniah, *Nature* **2019**, *570*, 363.
[13] J. Oh, D. Baek, T. K. Lee, D. Kang, H. Hwang, E. M. Go, I. Jeon, Y. You, C. Son, D. Kim, M. Whang, K. Nam, M. Jang, J.-H. Park, S. K. Kwak, J. Kim, J. Lee, *Nat. Mater.* **2021**, *20*, 385.
[14] J. B. Kim, C. Chae, S. H. Han, S. Y. Lee, S.-H. Kim, *Sci. Adv.* **2021**, *7*, 48.
[15] A. H. Dorrah, P. Bordoloi, V. S. de Angelis, J. O. de Sarro, L. A. Ambrosio, M. Zamboni-Rached, F. Capasso, *Nat. Photonics* **2023**, *17*, 427.
[16] C. He, Y. J. Shen, A. Forbes, *Light Sci. Appl.* **2022**, *11*, 205.
[17] A. H. Dorrah, F. Capasso, *Science* **2022**, *376*, abi6860.
[18] W. W. Liu, Z. C. Li, M. A. Ansari, H. Cheng, J. G. Tian, X. Z. Chen, S. Q. Chen, *Adv. Mater.* **2023**, *35*, 2208884.
[19] Y. J. Li, J. T. Hu, Y. X. Zeng, Q. H. Song, C. W. Qiu, S. M. Xiao, *Photonics Insights* **2024**, *3*, R03.
[20] V. J. Lloyd, S. L. Burg, J. Harizanova, E. Garcia, O. Hill, J. Enciso-Romero, R. L. Cooper, S. Flenner, E. Longo, I. Greving, N. J. Nadeau, A. J. Parnell, *Nat. Commun.* **2024**, *15*, 4073.
[21] V. Sharma, M. Crne, J. O. Park, M. Srinivasarao, *Science* **2009**, *325*, 449.
[22] Y. Chang, R. Middleton, Y.u Ogawa, T. Gregory, L. M. Steiner, A. Kovalev, R. H. N. Karanja, P. J. Rudall, B. J. Glover, S. N. Gorb, S. Vignolini, *Proc. Natl. Acad. Sci. U.S.A.* **2021**, *118*, 2111723118.
[23] D. Gur, A. S. Moore, R. Deis, S. Pang, X. Wu, I. Pinkas, C. Deo, N. Iyer, H. F. Hess, J. A. Hammer, J. Lippincott-Schwartz, *Proc. Natl. Acad. Sci. U.S.A.* **2024**, *121*, 2308531121.

[24] X. Q. Zhan, F. F. Xu, Z. H. Zhou, Y. L. Yan, J. N. Yao, Y. S. Zhao, *Adv. Mater.* **2021**, *33*, 2104418.
[25] S. U. Kim, Y. J. Lee, J. Q. Liu, D. S. Kim, H. H. Wang, S. Yang, *Nat. Mater.* **2022**, *21*, 41.
[26] J. Sandford O'Neill, P. Salter, Z. Zhao, B. Chen, H. Daginawalla, M. J. Booth, S. J. Elston, S. M. Morris, *Adv. Opt. Mater.* **2022**, *10*, 2102446.
[27] M. Zhang, Q.i Guo, Z. Li, Y. Zhou, S. Zhao, Z. Tong, Y. Wang, G. Li, S. Jin, M. Zhu, T. Zhuang, S.-H. Yu, *Sci. Adv.* **2023**, *9*, adi9944.
[28] Y. Chen, C. Zheng, W. Yang, J. Li, F. Jin, W. Zhang, W. Sun, P. Wang, L. Li, J. Wang, L. Jiang, *Adv. Mater.* **2025**, *37*, 2416448.
[29] J. Kobashi, H. Yoshida, M. Ozaki, *Nat. Photonics* **2016**, *10*, 389.
[30] R. Barboza, U. Bortolozzo, M. G. Clerc, S. Residori, *Phys. Rev. Lett.* **2016**, *117*, 053903.
[31] M. Rafayelyan, G. Tkachenko, E. Brasselet, *Phys. Rev. Lett.* **2016**, *116*, 253902.
[32] P. Chen, B. Y. Wei, W. Hu, Y. Q. Lu, *Adv. Mater.* **2020**, *32*, 1903665.
[33] L. Zhu, C.-T. Xu, P. Chen, Y.-H. Zhang, S.-J. Liu, Q.-M. Chen, S.-J. Ge, W. Hu, Y.-Q. Lu, *Light Sci. Appl.* **2022**, *11*, 135.
[34] K. Li, Y. Wang, D. Pi, B. Li, H. Luan, X. Fang, P. Chen, Y. Lu, M. Gu, *Opto-Electron. Adv.* **2024**, *7*, 230121,.
[35] S. Q. Liu, F. Fan, S. Z. Chen, S. C. Wen, H. L. Luo, *Laser Photonics Rev.* **2023**, *17*, 2300044.
[36] D. Zhu, Y.i-H. Zhang, S.i-J. Liu, W. Chen, L. Zhu, S.-J. Ge, P. Chen, W. Duan, Y.-Q. Lu, *Nano Lett.* **2023**, *24*, 140.
[37] L. Qin, X. Liu, K. He, G. Yu, H. Yuan, M. Xu, F. Li, Y. Yu, *Nat. Commun.* **2021**, *12*, 699.
[38] Y. Yang, X. Zhang, C. Valenzuela, R. Bi, Y. Chen, Y. Liu, C. Zhang, W. Li, L. Wang, W. Feng, *Matter* **2024**, *7*, 2091.
[39] R. Lan, J. Bao, Z. Li, Z. Wang, C. Song, C. Shen, R. Huang, J. Sun, Q. Wang, L. Zhang, H. Yang, *Angew. Chem. Int. Ed.* **2022**, *134*, 202213915.
[40] K. Y. Bliokh, F. J. Rodríguez-Fortuño, F. Nori, A. V. Zayats, *Nat. Photonics* **2015**, *9*, 796.
[41] A. Ryabchun, O. Sakhno, J. Stumpe, A. Bobrovsky, *Adv. Opt. Mater.* **2017**, *5*, 1700314.
[42] C. W. Chen, I. C. Khoo, *Proc. Natl. Acad. Sci. U.S.A.* **2021**, *118*, 2021304118.
[43] Y.-H. Zhang, S.-J. Liu, P. Chen, D. Zhu, W. Chen, S.-J. Ge, Y. Wang, Z.-F. Zhang, Y.-Q. Lu, *Nat. Commun.* **2024**, *15*, 1108.
[44] Y. Bao, Y. Yu, H. Xu, C. Guo, J. Li, S. Sun, Z.-K. Zhou, C.-W. Qiu, X.-H. Wang, *Light Sci. Appl.* **2019**, *8*, 95.
[45] M. Song, L. Feng, P. Huo, M. Liu, C. Huang, F. Yan, Y.-Q. Lu, T. Xu, *Nat. Nanotechnol.* **2022**, *18*, 71.